Influence of Diffraction Coefficient and Corner Shape on Ray Prediction of Power and Delay Spread in Urban Microcells

Hassan M. El-Sallabi, *Student Member, IEEE*, George Liang, *Member, IEEE*, Henry L. Bertoni, *Fellow, IEEE*, Ioannis T. Rekanos, *Member, IEEE*, and Pertti Vainikainen, *Member, IEEE*

***Abstract*—For a low base-station (BS) antenna located on one street, signals propagate into crossing and parallel streets by reflection and diffraction at corners of buildings. Therefore, in order to accurately predict the received signals, it is necessary to properly model the diffraction coefficient at the building edge and to accurately represent the shape and the electrical properties of the building near the corner. This paper compares ray-tracing predictions to measurements of received power and root mean square (rms) delay spread and shows the need for a diffraction coefficient having larger values than suggested by the commonly used heuristic diffraction coefficient. A new heuristic diffraction coefficient is proposed that has higher diffracted field strength in the deep shadow region and in the region between the two shadow boundaries. The proposed diffraction coefficient shows better agreement with measurements of both received power and delay spread compared to the commonly used heuristic diffraction coefficient. The influence of building shape near the corner and its electrical properties on the ray-tracing predictions are also presented. The shape is shown to have an important role in accurately predicting both received power and delay spread.**

***Index Terms*—Heuristic diffraction coefficient, ray prediction, microcellular environment.**

I. Introduction

THE DEPLOYMENT of high-speed digital communication systems in urban environments will place new demands on propagation models. Developed propagation models should accurately predict the amplitude, delay, and direction of arrival of multipath echoes created by the propagation environment, which are important parameters for new broad-band communication systems. The most common modeling approach is ray tracing, which is based on geometric optics. Recently, ray-tracing techniques have been used for the prediction of multipath components in site-specific scenarios [1]–[9].

The accuracy of ray tracing depends on the physical processes that are taken into account and the accuracy of buildings database. Reflection and diffraction are the main physical processes that are considered in outdoor ray tracing algorithms. For low BS antennas, reflection near building corners and diffraction at the corners are important in diverting the radio signals into shadowed regions. Near the corner, reflected rays give the dominant contribution, while far from the corners the diffracted rays are the most dominant. Thus, accurately modeling building corners, such as that shown in Fig. 1, is important for predicting the signal characteristics in the shadow regions. Moreover, the choice of the diffraction coefficient is important for predicting the signal amplitude far from the corner.

Fig. 1. Picture of a building corner.

Diffraction formulas are well established for perfectly conducting infinite wedges through the uniform theory of diffraction (UTD) [10], [11], for absorbing wedges [12], and for nonperfectly conducting surfaces [13]–[16]. Many of the impedance-surface diffraction formulas are based on Maliuzhinets' solution [17] and are rather cumbersome to use for propagation prediction in mobile communications. Thus, the difficulty of using the rigorous solutions for propagation prediction forces simplifications to be made. In order to treat diffraction over hills and mountains, Luebbers [18] modeled them as dielectric wedges by heuristically modifying the

Manuscript received June 21, 2001; revised March 6, 2002. This work was supported by the Helsinki University of Technology (HUT), the Academy of Finland, and in part by the Center for Advanced Technology in Telecommunications (CATT) at Brooklyn Polytechnic University, NY.

H. M. El-Sallabi, I. T. Rekanos, and P. Vainikainen are with the Radio Laboratory, Helsinki University of Technology, FIN-02015, Espoo, Finland (e-mail: hsallabi@cc.hut.fi).

G. Liang is with the EMAG Technologues Inc., Ann Arbor, MI 48108 USA.

H. L. Bertoni is with the Department of Electrical Engineering, Polytechnic University, Brooklyn, NY 11201 USA.

Publisher Item Identifier S 0018-926X(02)05460-1.

perfectly conduction UTD diffraction coefficient [10], [11]. The problem with Luebbers' heuristic diffraction coefficient (LHDC) is that it is small in the region between the two shadow boundaries, and that it has a deep null in the illuminated region that does not appear to have a physical basis. As a result, amplitude predictions made by using the LHDC in the aforementioned regions are low. In [19], [20] an improvement of Luebbers' diffraction coefficient is made to eliminate the dip in the diffracted field in the lit region but it is not clear if the presented definition of reflection angles is universal. Holm [21] has proposed a further modification of the LHDC. However, this modification does not address the value of the diffraction coefficient inside the illuminated region and the null found for the LHDC. In addition, the diffracted field is still low in the region between the two shadow boundaries.

As applied to diffraction at building corners, it may not be realistic to even model the corner as an impenetrable wedge. The internal structure of the walls near the corner, as well as penetration through windows near the corner, render all of the forgoing diffraction coefficients invalid. One realization of a building corner is analyzed using the finite-difference time-domain (FDTD) method [22]. The FDTD diffraction coefficient is indeed larger than that of Luebbers' over the range of diffraction angle of importance for turning corners in urban canyons. In this work, we propose a simple new heuristic diffraction coefficient (NHDC) in order to gain the benefit of the larger diffracted amplitude predicted by the absorbing wedge diffraction coefficient [12] for glancing rays, and yet makes the total field continuous at reflection shadow boundaries [10]. The NHDC overcomes both problems that appear when the LHDC is used, i.e., the artificial dips and the low value in diffracted signal strength. A set of wide-band measurements of amplitude and delay spread made in Helsinki are used to evaluate and compare the predictions made using the new heuristic diffraction coefficient and those made with LHDC.

The formulation of the diffraction coefficient is presented in Section II. An overview of the vertical plane launch ray tracing algorithm used in predictions is given in Section III. The wide-band measurement system and the measurements made in Helsinki, which are used for comparison, are described in Section IV. Section V discusses the influence of the diffraction coefficient on the predictions and presents the comparison between predictions and measurements of both received power and rms delay spread. The influence of the building corner shape on the prediction of these parameters is described in Section VI.

II. Dielectric Wedge Diffraction Coefficient

When the source and observation points are both in the plane perpendicular to an edge, the diffracted electric field is given by

$$E_{\text{diff}} = E_i D(\phi, \phi') \sqrt{\frac{\rho'}{\rho(\rho+\rho')}} e^{-jk\rho} \tag{1}$$

where E_i is the incident field at the edge. The terms ρ' and ρ represent the distance from the source to the edge and from the edge to the observation point, respectively, as shown in Fig. 2. The term $D(\phi, \phi')$ is the UTD diffraction coefficient, which depends on the angles ϕ and ϕ' between one face (usually 0-face) of the wedge and the observation point and source point, respectively.

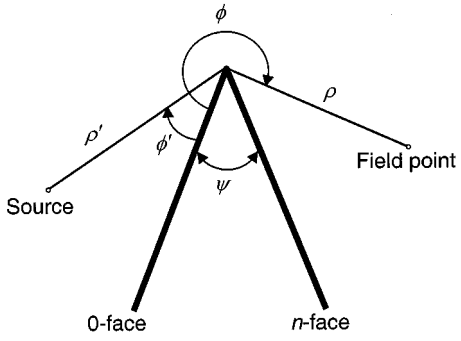

Fig. 2. Ray geometry for diffraction by a wedge.

Luebbers introduced a heuristic modification to the UTD diffraction coefficient (for a conducting wedge) to be applicable to finite conductivity dielectric wedges in order to make the fields continuous across the shadow boundaries. He identified two of the four terms in the diffraction coefficient of the perfectly conducting wedge [10] and multiplied them by the plane wave Fresnel reflection coefficient. He conjectured that this approach would yield a reliable estimate for the diffraction coefficient, particularly, around the incidence and reflection shadow boundaries. LHDC is applicable when the wedge interior angle is large, the observation point lies near the shadow boundary, and the observation angles are larger than the angles of incidence [19]. Detailed formulation of the LHDC can be found in [18].

The LHDC is plotted in Figs. 3(a) and (b) for the cases when the source can see one or both faces of a right angle wedge, respectively. For low antennas oriented for vertical electric field, the field is nearly parallel to the vertical building corners. Thus, the plots in Fig. 3 are made assuming the transverse electric (TE) polarization. The diffraction coefficient has a peak at the shadow boundary of the incident and reflected waves in Fig. 3(a) and at the reflection shadow boundaries in Fig. 3(b). The figure shows that the diffraction coefficient has a null for ϕ to the left of the shadow boundary and is small in the region between the two peaks which occur at the two shadow boundaries. The null does not appear to have a physical basis. It seems to come from the mathematical formulation. We have also plotted in Fig. 3 the diffraction coefficient for a wedge with absorbing faces [12]. The coefficient magnitude has a peak at the incident wave shadow boundary, but none at the reflection shadow boundaries. However, it is larger than Luebbers' coefficient for rays glancing along the face of the wedge, which are responsible for the received signal at distances far from the corner.

In order to gain the benefit of the larger diffracted amplitude predicted for glancing rays by the absorbing coefficient, and to preserve the continuity of the total filed at the reflection shadow boundary, we propose a new heuristic diffraction coefficient. The proposed NHDC is given by

$$D(\phi, \phi') = -\frac{1}{\sqrt{2\pi k}} \times \begin{pmatrix} (\pi - |\phi - \phi'|)^{-1} \cdot F[kLa^-(\phi - \phi')] \\ +(\pi + |\phi - \phi'|)^{-1} \cdot F[kLa^+(\phi - \phi')] \end{pmatrix} \tag{2}$$

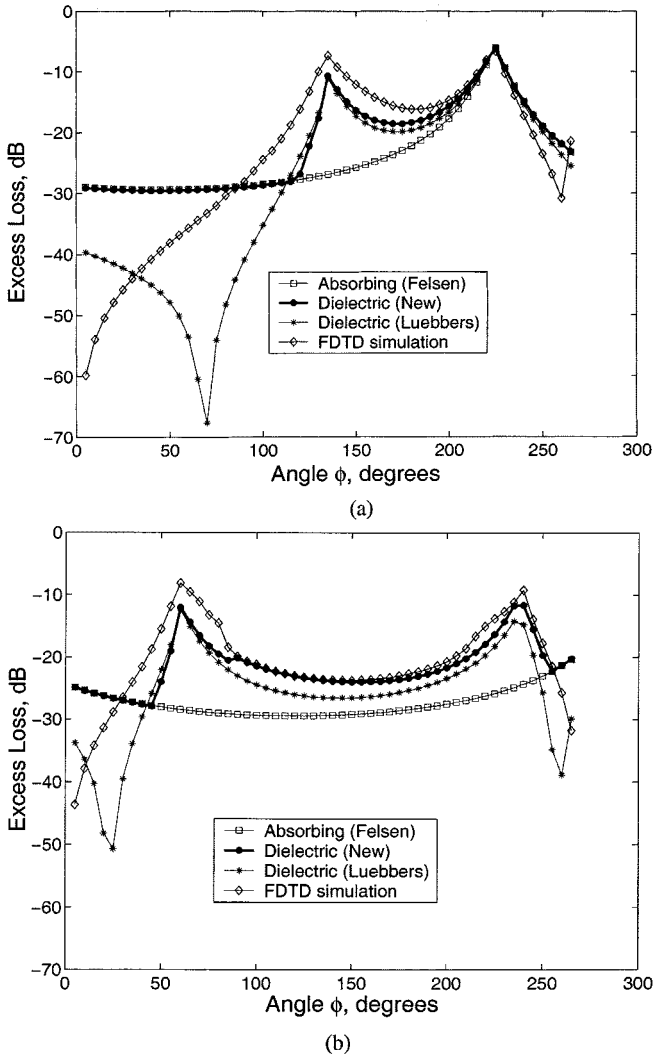

Fig. 3. Comparison of diffraction coefficient for a 90° dielectric wedge ($\varepsilon_r = 5, \sigma = 0.005$ S/m) for source and receiver at a distance $\rho = 3$ m. (a) $\phi' = 45°$. (b) $\phi' = 120°$.

or by (3)given at the bottom of the page; whichever is greater in magnitude. The angles ϕ' and ϕ are the incident and diffracted ray angles with respect to the illuminated face of the wedge and n is related to the internal angle of the wedge ψ by the relation $\psi = (2-n)\pi$.

Equation (2) is just the diffraction coefficient for an absorbing wedge and includes only the incidence shadow boundary. The two additional terms in (3) are added heuristically in this work to represent the reflection shadow boundary, which does not exist in Felsen's diffraction coefficient for an absorbing wedge [12]. The functions $F(kLa^{\pm}(\phi \pm \phi'))$ are related to the complementary error function, and are defined in [10], [11], [18]. These functions are responsible for making the field continuous across the shadow boundaries. The reflection coefficients are given by

$$\Gamma_{0,n} = \frac{\cos\theta_i - a_p \cos\theta_t}{\cos\theta_i + a_p \cos\theta_t} \tag{4}$$

where a_p is $\sqrt{\varepsilon_r}$ for parallel polarization and is $1/\sqrt{\varepsilon_r}$ for perpendicular polarization of the electric field. The angles of incidence θ_i and refraction, θ_t are measured with respect to the normal of the wedge face 0 or n.

The magnitude of the NHDC for a right-angle wedge and for TE polarization is plotted in Fig. 3. It is seen that this coefficient is equal to or greater than the LHDC for almost all values of ϕ, including angles in the regions between the two shadow boundaries. Moreover, the new diffraction coefficient is much stronger for ϕ approaching 90° when $\phi' = 45°$ [Fig. 3(a)] and somewhat stronger for small angles ϕ when $\phi' = 120°$ [Fig. 3(b)]. These conditions are significant for coupling energy from the line-of-sight (LOS) street into a cross street at an intersection of the four building corners. In this case, the strongest diffraction contributions to the coupling come from the building corner whose two faces are visible from both the LOS street and the side street. Diffraction at this corner corresponds to Fig. 3(b) with ϕ lying between the two shadow boundaries. Because the NHDC is larger than Luebbers' coefficient, the use of the NHDC will substantially increase the predicted signal.

In order to further justify the use of the NHDC, we have considered one realistic type of building corner and have computed the diffraction coefficient using the FDTD method. The building corner assumed for this simulation is a hollow dielectric wedge having wall thickness of 0.5 m, with a square conducting post embedded in the corner to represent a structural element in the building frame. A dielectric relative permittivity of 5 and conductivity of 0.005 S/m at frequency of 900 MHz were assumed for the walls. Using the FDTD, we calculate the field at 53 points uniformly distributed on an arc $(0° \le \phi \le 270°)$ of radius equal to 3 m and centered at the building corner. The simulation results are processed in order to obtain the diffracted field from the total field. The FDTD diffraction coefficient is also plotted in Fig. 3. The abrupt increase at 265° is due to our inability to separate the diffracted field from the field transmitted through the building walls. Fig. 3 illustrates that in the illumination region before the first shadow boundary, the FDTD coefficient has its own variation, but is larger than Luebbers' coefficient over most of the range of ϕ. However, for ϕ in the important region between the two shadow boundaries, i.e., between the peaks, the FDTD diffraction coefficient is nearly equal to the NHDC. Other corner constructions will lead to somewhat different diffraction coefficients, and deserve further study. However, comparisons of measurements with ray predictions, which are discussed below, further confirm the need to use a diffraction coefficient having larger values than those predicted by the LHDC.

$$D(\phi,\phi') = -\frac{1}{\sqrt{2\pi k}} \begin{pmatrix} (\pi - |\phi - \phi'|)^{-1} \cdot F[kLa^{-}(\phi - \phi')] \\ +(\pi + |\phi - \phi'|)^{-1} \cdot F[kLa^{+}(\phi - \phi')] \\ +\Gamma_0[\pi - (\phi + \phi')]^{-1} \cdot F[kLa^{-}(\phi + \phi')] \\ +\Gamma_n[\phi + \phi' - (2n-1)\pi]^{-1} \cdot F[kLa^{+}(\phi + \phi')] \end{pmatrix} \tag{3}$$

III. The Vertical Plane Launch (VPL) Algorithm

The vertical plane launch (VPL) method [3], [4] is a robust three-dimensional (3-D) ray-tracing technique that can compute the multiple arriving rays in a heterogeneous building environment for base-station antennas located at any height. The VPL approach accounts for specular reflections from vertical building surfaces and diffraction at vertical edges and approximates diffraction at horizontal edges by restricting the diffracted rays to lie in the plane of incidence, or in the plane of reflection. This approximation allows the rays to be found by first applying the shooting and bouncing ray approach in the horizontal plane to find the vertical planes, followed by analytical construction of the vertical ray path in the unfolded vertical plane. As a result, the VPL code runs significantly faster than the full 3-D computer codes. When unfolded, each vertical plane contains two rays, one that reaches the mobile directly and one that is reflected by the ground. The fields of these rays are added coherently.

In the version used for this study, the VPL method neglects rays that are transmitted through the building, diffuse scattering from the walls, and rays that travel under a structure. The received power delay profile for a pulsed source can be predicted by individual versions of the transmitted pulse, delayed according to the ray path length and weighted by the ray field amplitude. The statistical properties of the delay profiles can be obtained from ray simulations. Details of the VPL algorithm can be found in [3].

IV. Helsinki Measurements

A measurement campaign was carried out in the city center of Helsinki, Finland. Fig. 4 shows the measurement environment and routes over which the transmitter is moved. The average height of the surrounding buildings is about 25 m. The routes in Fig. 4 are designed to measure microcell coverage for distance less than 1 km using antennas that are low compared to the surrounding buildings. For future broad-band systems and networks, the received power and rms delay spread are parameters of concern and will be discussed here. Cell coverage and interference analysis are correlated with received power. Meanwhile, the maximum data rate is directly related to the rms delay spread.

The measurement system is based on a linear array of 15 dual-polarized antenna elements, slanted $\pm 45°$, with spacing of 0.7λ between elements [23], and a complex wide-band radio channel sounder [24]. A wide-band signal is transmitted using a single mobile antenna, and received separately with each of the 15 antenna elements and both polarizations, using a fast radio frequency switch. The carrier frequency of the sounder is 2.154 GHz and the receiver bandwidth is 100 MHz. A chip frequency of 30 MHz is used for a pseudo random (PN) modulating sequence of length of 127 in the transmitter, resulting in delay resolution of 33 ns. In the receiver, the demodulated signal is divided into phase I- and quadrature Q-branches and sampled with two 120 Msps analog-to-digital (A/D)-converters. The signal samples from each branch of the switch are then stored for off-line processing to obtain the complex impulse response (IR) of the channel corresponding to each element and

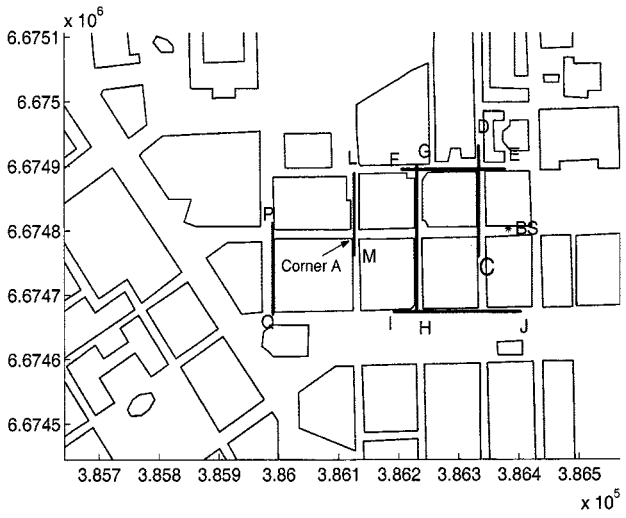

Fig. 4. Microcellular measurement environment with measuring routes.

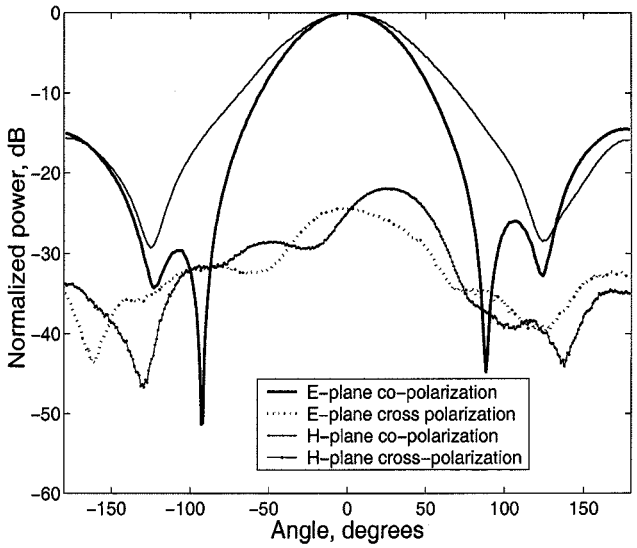

Fig. 5. Radiation pattern of a base-station antenna element.

polarization. Each element of the array is a stacked microstrip patch antenna having two separate feeds for orthogonal polarizations with high cross-polarization discrimination (XPD) and sufficient bandwidth to meet the requirement of the measurement system. Fig. 5 presents the radiation pattern of one element. The 3-dB beamwidth of the element is about 60° in the E-plane and about 70° in the H-plane. The XPD is higher than 20 dB within the 3-dB beamwidth. The measured gain of the element is about 7 dBi. The transmitter antenna is an omnidirectional discone with gain of 2 dBi, vertical polarization, and 40 dBm radiated power.

The route types shown in Fig. 4 are LOS and out-of-sight (OOS), which includes both perpendicular and parallel streets. The routes C–D, G–H, L–M, and P–Q shown in Fig. 4 represent different side streets that cross the LOS street with the receiver array, which is shown as the BS. The routes E-F and I–J represent parallel streets at both sides of the LOS street. The transmitter is placed on a trolley with the antenna of a height of 1.8 m, and is moved over the measurement routes at an approximate speed of 1.1 m/s. The linear antenna array at the BS are located

at heights of 3, 8, and 13 m. The measurement results presented here are only for BS height of 3 m.

Two IRs were averaged from each channel to reduce the effect of switching between the antenna elements. The IRs from each element and polarization were recorded at a rate of approximately 5 IRs per moved wavelength (~ 0.14 m) at the given speed. To avoid nonstationarity of the channel, the whole measurement campaign was carried out at night with no traffic. The measured complex IRs of each element are obtained from the $\pm 45°$ slanted microstrip antennas. The complex IRs of the two polarizations are off line processed by vector addition to produce the vertically polarized signals. The vertically polarized power delay profiles are averaged spatially over antenna elements and over a distance of λ to remove any fast fading. The processed data are used to obtain both the wide-band received power and rms delay spread.

V. Comparison of Measurements With NHDC and LHDC Prediction

Comparisons between measurement results and prediction of the VPL algorithm using both the NHDC and LHDC are made for the received power and the rms delay spread. For all prediction results shown here, the same simulation parameters are used. Reflection at building walls is modeled by the Fresnel reflection coefficient using the permittivity $\varepsilon_r = 5$. This value is consistent with the range $\varepsilon_r \approx 5$–7 suggested by direct measurements [25]. For all predictions, rays are traced up to the seventh order of reflection and including a single vertical corner diffraction for receivers in cross streets, but allowing for double vertical corner diffraction for receivers in parallel streets.

A. Wide-Band Received Power

For a PN probe signal, the spatially averaged wide-band received power for a measured power delay profile can be calculated as presented in [26], [27]. In order to maintain the site-specific information in the measurement results as much as possible and remove the fast fading, the measurement data are processed to obtain a local mean power in steps of 0.5 m along the traveling route. The obtained mean measured power is compared to the mean predicted power. The predicted mean power is computed with a spatial resolution of 0.5 m since it is calculated as the sum of powers of the rays reaching the receiver, which is inherently the spatial average.

1) Received Power in Perpendicular Streets: Fig. 6 depicts the measured and predicted mean power for routes C–D, G–H, and P–Q on perpendicular streets. Route C–D is at the end of the block having the BS. In Fig. 6(a) the received mean power is close to -30 dBm in the LOS region, but it drops by about 20 dBm in near shadow regions, and a further 25 dBm far from the corner. Fig. 6(a) shows that the rate of power decrease is higher in the near shadow region where reflected rays dominate than in the deep shadow regions where the diffracted rays give dominant contribution. The predictions with the NHDC generally follow the measurements better than when LHDC is used. However, at distances beyond 120 m the measured power is lower compared to the power predicted by the NHDC. This may result from an error in modeling the large (about 15-m) colonnade entrance to a building by a flat surface in the building database. The mean error between the measurements and the VPL

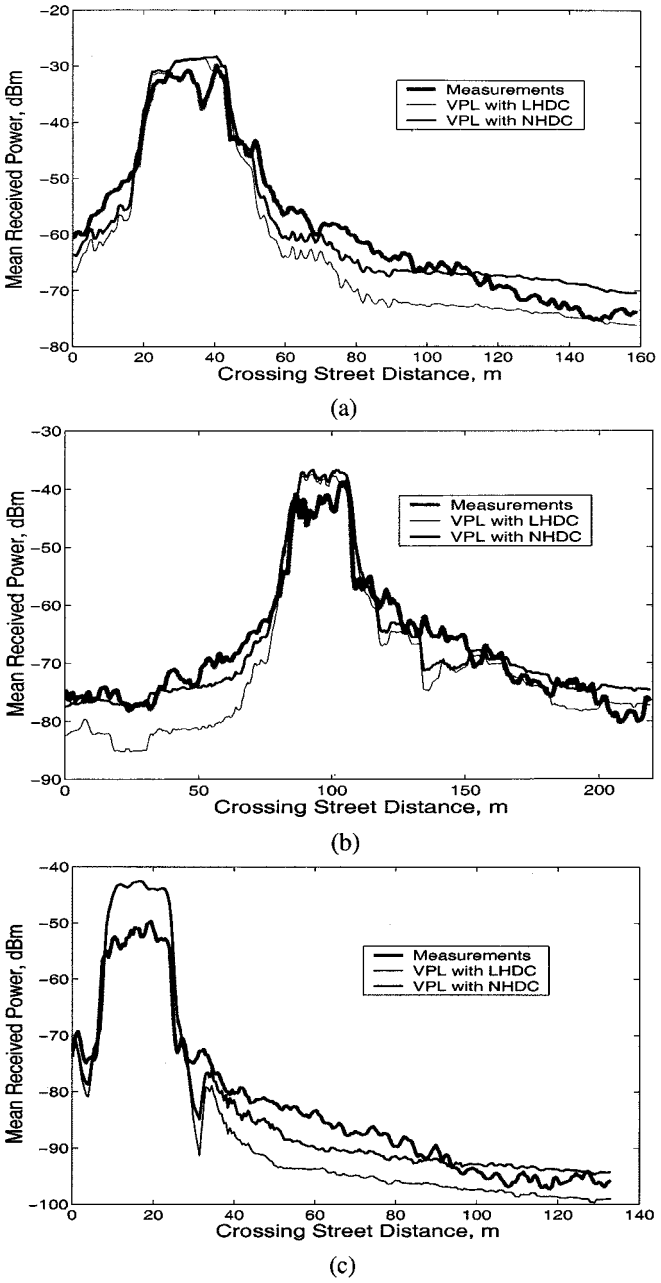

Fig. 6. Power comparison of VPL with NHDC and LHDC versus measurements when mobile travels along perpendicular streets. (a) Route C–D. (b) Route G–H. (c) Route P–Q.

with the NHDC is about 0.1 dB, and the standard deviation is about 3.7 dB. These values are lower than those obtained from the VPL with LHDC (see Table I).

Fig. 6(b) shows the corresponding comparison for route G-H. The maximum received power along the route is -39 dBm in the LOS region, with a minimum value of about -80 dBm in the deep shadow region. Fig. 6(b) depicts that the rate of power decrease from LOS to OOS is higher than that of the route C–D, which can be explained as follows. Since the distance from the BS to the intersection of the route G–H is larger than that of the route C–D, the direct rays to the BS span a narrower range of angles. These rays are generated by rays that are multiply reflected between the buildings on the side street. For route G–H, the rays on the side streets are more nearly perpendicular to the

TABLE I
SUMMARY OF POWER AND RMS DELAY SPREAD PREDICTION ACCURACY FOR COMPARISON BETWEEN THE TWO DIFFRACTION COEFFICIENTS

	POWER				DELAY SPREAD			
	VPL/NHDF		VPL/LHDF		VPL/NHDF		VPL/LHDF	
ROUTE	Mean (dB)	Std (dB)	Mean (dB)	Std (dB)	Mean (ns)	Std (ns)	Mean (ns)	Std (ns)
C-D	0.06	3.67	-3.94	4.06	-12.52	17.48	-17.83	20.28
G-H	2.56	3.41	-0.72	4.88	7.82	19.97	5.64	19.28
P-Q	-0.26	4.58	-3.95	5.82	-15.18	15.12	-18.75	17.12
E-F	0.07	3.48	-5.77	3.43	5.13	134.27	-17.78	111.89
I-J	4.12	3.85	2.53	3.82	-23.59	81.43	55.87	113.33

buildings than that of the route C–D, so that more reflections are required for the same distance from the corner and hence, the signal falls more rapidly in going from LOS to OOS locations. This difference is seen by comparing the slope of transition in power from LOS to OOS locations in Figs. 6(a) and (b). Fig. 6(b) shows that the predictions with the NHDC generally follow the measurements and is closer than the predictions with the LHDC, especially for locations in the range from 0 to 80 m. The mean value of the prediction error of the VPL with NHDC is about 2.56 dB and the standard deviation is 3.41 dB. The mean is higher than the corresponding value of LHDC but the standard deviation is lower (see Table I).

The comparison of results for route P–Q, which is about 400 m from the BS, is depicted on Fig. 6(c). Route P–Q has the sharpest power transition from LOS to OOS as compared to all the previous side streets. The mean prediction error of VPL with NHDC for this route is about -0.3 dB and the standard deviation is about 4.6 dB, which are both smaller than their corresponding values obtained with LHDC (see Table I). It is clear that the predictions using the VPL with LHDC underestimates the measurements.

2) Received Power in Parallel Streets: Fig. 7 shows comparison results for routes E–F and I–J on parallel streets with respect to the LOS street of the BS. The comparison results for route E–F in Fig. 7(a) show that the VPL predictions using NHDC follow the measurement results quite well, in contrast to the predictions obtained with LHDC. From the mean and standard deviation given in Table I, it is seen that the mean error using NHDC is much lower than that when using LHDC. As shown in Fig. 7(b), for the route I–J, both the LHDC and the NHDC give similar results. On route I–J, there is a row of trees in leaf in the middle of the street from 0 to about 150 m. This may explain why the measured power is lower than the predicted power when the mobile is away from the crossing street junction, since rays bouncing between the two sides of the parallel street will experience more attenuation due to the trees. In general, the comparisons for all routes indicate that the VPL with the NHDC provides better agreements with measurement results.

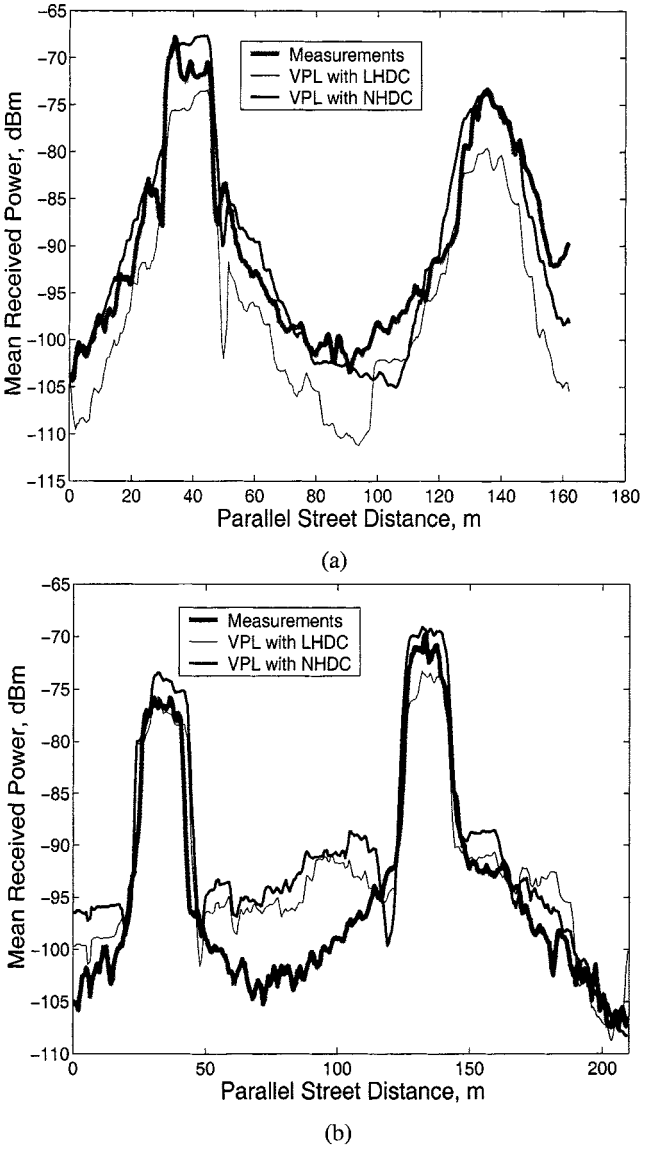

Fig. 7. Power comparison of VPL with NHDC and LHDC versus measurements when mobile travels along parallel streets. (a) Route E–F. (b) Route I–J.

B. RMS Delay Spread

Dispersion in the delay domain is an important phenomenon, which is usually measured by the rms delay spread. It has a significant effect on the design of communication systems. This section presents a comparison between predicted and measured

TABLE II
SUMMARY OF MEASURED RMS DELAY SPREAD IN ALL ROUTES

ROUTE	MEASUREMENTS			
	Mean (ns)	Std (ns)	Min (ns)	Max (ns)
C-D	45.4	23.5	9.5	101.9
G-H	41.3	15.0	9.6	86.3
L-M	27.1	15.8	9.4	96.1
P-Q	51.0	22.6	9.5	134.5
E-F	114.1	103.3	9.5	627.9
I-J	100.5	53.8	12.6	251.2

results of rms delay spread. The predictions are obtained using the VPL tool with LHDC and NHDC. For the sake of comparison, it is necessary that the predicted power-delay profiles have the same time resolution of the measurement system. In order to achieve this, each arriving ray is assumed to have a time dependence that is delayed version of the PN m-sequence used in the measurement system. The arriving multipath rays are then added coherently in each time bin. As a consequence of this summation, the shape of the resultant power delay profile (and hence the rms delay spread) is a function of the phase of many individual arriving rays.

The phenomenon described above is also observed in measurements of power during time delay bins due to coherent addition of multipath arrivals. As a result, the rms delay spread obtained from measurements shows a wide range of fluctuation from one point to the next along a measurement route. The statistics of the variation in rms delay spread along the various measurement routes is listed in Table II. The minimum value of rms delay spread is almost the same for all routes and is related to system resolution, while the maximum values are about nine or more times the minimum values. On the heavily shadowed parallel streets, the mean value of delay spread is about two times greater than the mean value on the cross streets, and the maximum delay spread shows even greater variation.

It is not reasonable to expect propagation models to produce better agreement with measurements than that obtained between identical measurements in the same location. Repeating the measurements over the same route after a few minutes shows large differences in rms delay spread at the same point on the route [2]. Thus, in order to remove the phase uncertainty, the rms delay spread calculated from averaged measured power delay profiles are processed to obtain mean rms delay spread at 0.5-m-separated points for comparison with prediction. The calculation of the rms delay spread is carried out by using the well known second central moment approach [28].

Figs. 8 and 9 depict comparison between measured and predicted mean rms delay spread for perpendicular and parallel streets on routes C–D, G–H, P–Q, and routes E–F, I–J, respectively. In Fig. 8(a), the rms delay spread beyond the distance of 110 m increases more than predicted, this may be due to large electrical irregularity of the building entrance which causes diffuse scattered rays that results in wider excess delay paths with lower amplitude that results in higher rms delay spread and

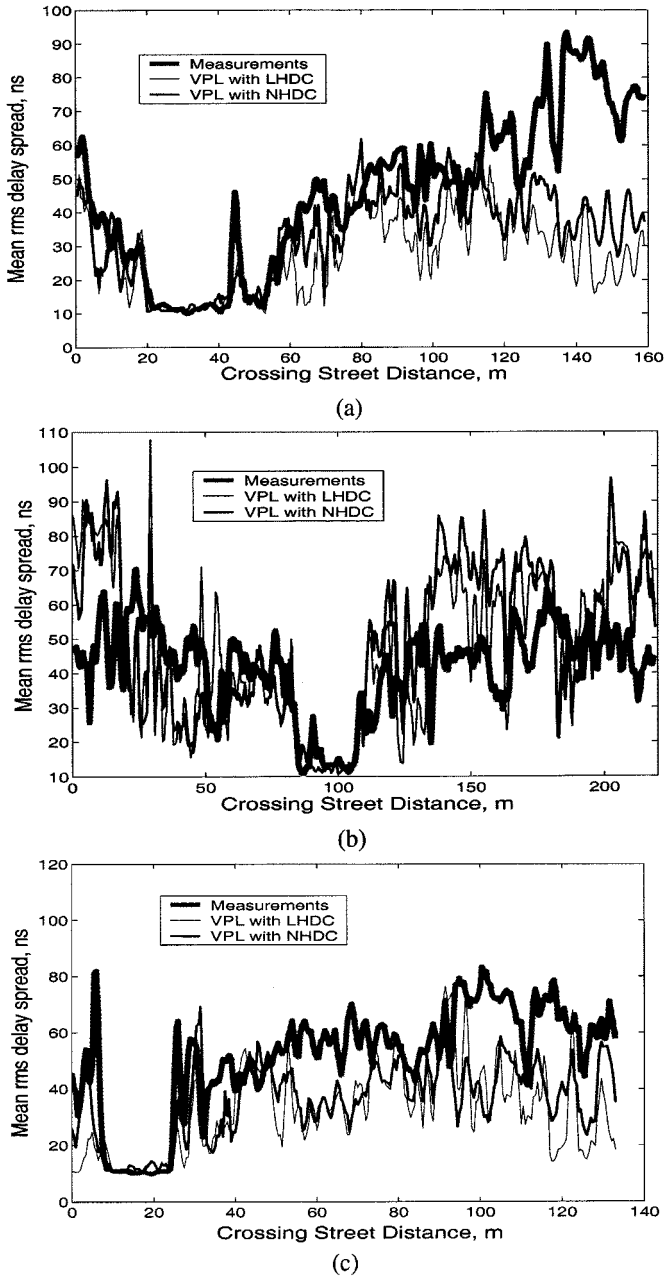

Fig. 8. Delay spread comparison of VPL with NHDC and LHDC versus measurements when mobile travels along perpendicular streets. (a) Route C–D. (b) Route G–H. (c) Route P–Q.

lower received power as noted in Fig. 6(a). It is seen from Figs. 8 and 9 that there can be considerable differences in the delay spread obtained with LHDC and NHDC, and considerable difference between either of them and the delay spread obtained from measurements. Since the VPL prediction with LHDC and NHDC use different diffraction coefficients and the VPL has a threshold for excluding rays that have amplitude of X decibels ($X = 20$ dB in this work) lower than the maximum, the found number of rays is higher and the path lengths are different for the case when the NHDC is used. This is reasonable because the NHDC predicts higher amplitude compared to the LHDC. Thus, different power-delay profiles are predicted with different diffraction coefficient. As a result different rms delay spread are predicted. Table I shows the mean and standard deviation of

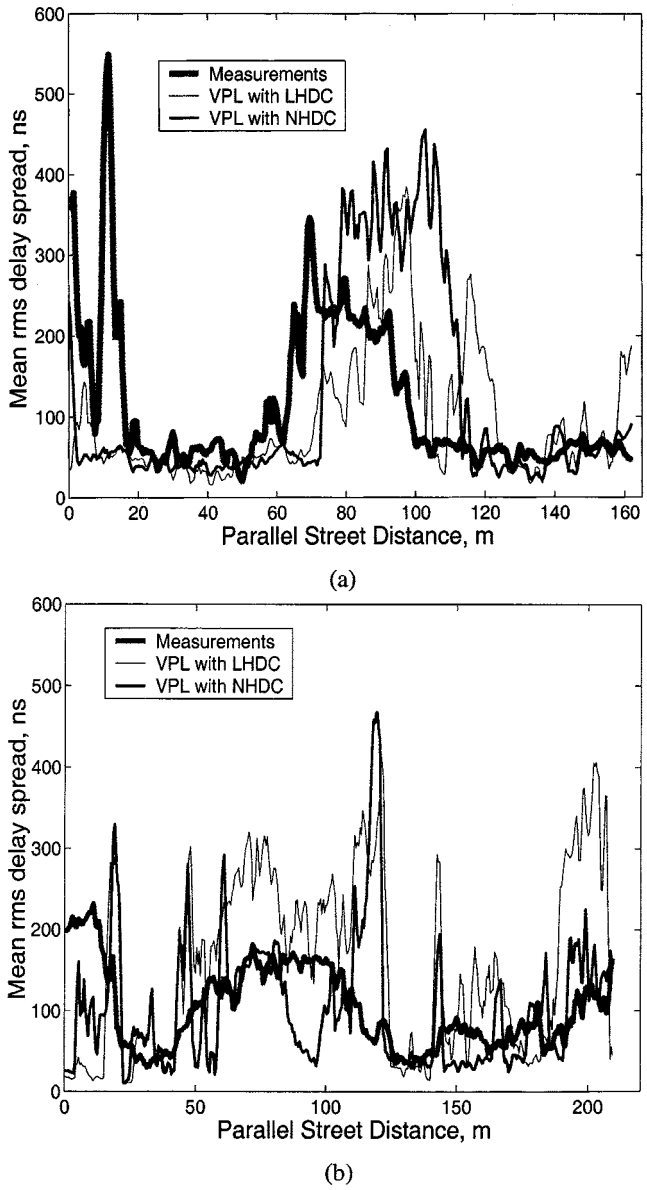

Fig. 9. Delay spread comparison of VPL with NHDC and LHDC versus measurements when mobile travels along parallel streets. (a) Route E-F. (b) Route I-J.

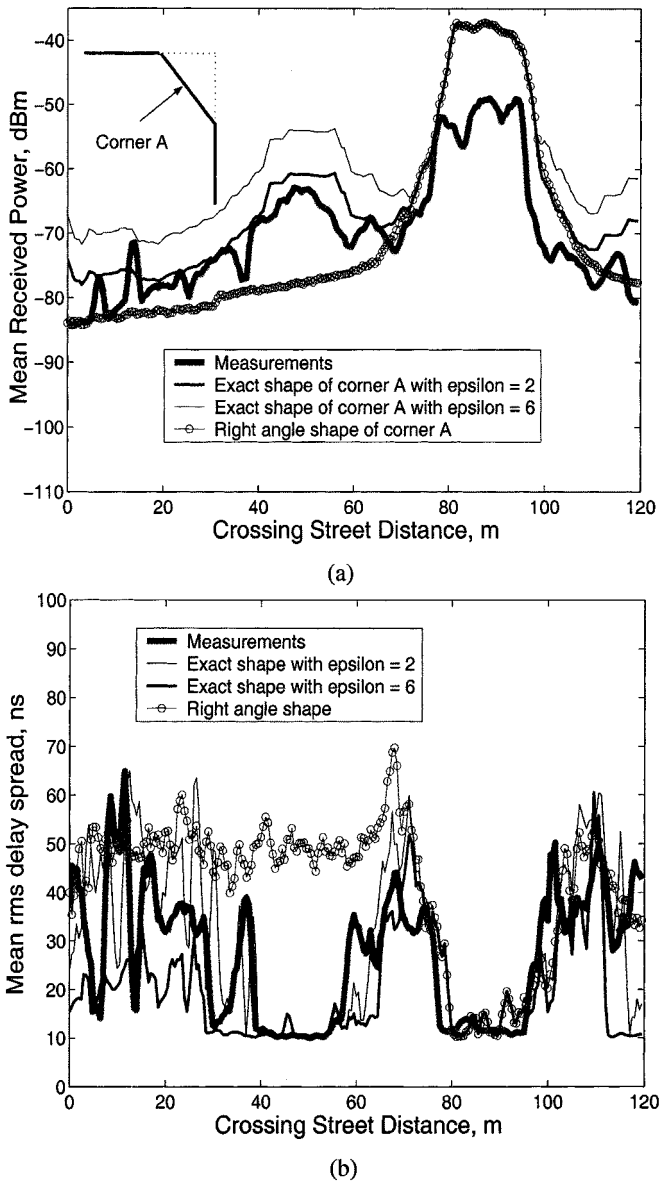

Fig. 10. Effect of the shape and the properties of corner A on a the prediction along the route L–M. (a) Power. (b) Delay spread.

prediction errors on different routes. Generally, the prediction of VPL with NHDC gives slightly better agreement with measurements than the VPL with LHDC, although, the statistical difference between the delay spreads found using the two alternative diffraction coefficients not as significant as that observed in power predictions.

VI. Influence of Corner Shape

The influence of database inaccuracy on path loss predictions was investigated in [29]. It was shown that some of the details of each building block, especially openings between buildings are important for accurate predictions. It was also found that the predictions are more sensitive to errors in the location of building corners than to errors in the building size. To the authors knowledge, there is no comparative work that studies the effects of the inaccuracy of the database on the rms delay spread. In this section, the emphasis will be on the shape of the building corners and their electrical properties, since they are usually modeled by right angle wedge but may have a different shape.

Fig. 1 shows a picture of the corner labeled A in Fig. 4. The solid and dotted lines of the insert in Fig. 10(a) represent the real shape and the usually assumed right angle corner shape, respectively. The comparison of measurements made on route L–M to predictions made using the VPL with NHDC are given in Fig. 10. The curves in Fig. 10 depict the received power and rms delay spread along the route L–M, found from the measurements and predicted using the two shapes of corner A. As can be seen in Fig. 1, the corner has a flat surface rather than sharp corner. Actually, the flat surface reflects the signal onto the long segment of route L–M. Modeling the corner by a 90° wedge implies that the corner acts as a diffracting edge, which results in predicted signal amplitude that is smaller than measured, as seen in Fig. 10(a).

TABLE III
SUMMARY OF POWER AND RMS DELAY SPREAD PREDICTION OF ROUTE L–M UNDER DIFFERENT PROPERTIES OF THE CORNER A in FIG. 4

	POWER		DELAY SPREAD	
ROUTE L-M	Mean (dB)	Std (dB)	Mean (ns)	Std (ns)
Exact shape with $\varepsilon_r = 2$	5.41	4.64	2.81	13.26
Exact shape with $\varepsilon_r = 6$	10.29	3.71	-7.20	12.28
Right angle shape	-0.45	8.38	14.38	15.45

As shown in Fig. 1, the reflecting surface of the corner consists basically of glass. For the low BS antennas discussed here, it is the doors and window above them that are responsible for the reflections. If the reflection coefficient for this wall is computed with $\varepsilon_r = 6$, as used for all other walls, the prediction highly overestimates the signal, as shown in Fig. 10(a). By selecting a lower value of permittivity $(\varepsilon_r = 2)$ for this surface only, and setting $\varepsilon_r = 6$ for the other surfaces, we obtain better agreement with measurements. The mean value of the prediction error of the VPL with NHDC and reflective surface with $\varepsilon_r = 6$ is about 10.3 dB, which is much higher than that with $\varepsilon_r = 2$. However, the standard deviation of the former is slightly lower (see Table III). The transition slope of power decrease from LOS to OOS is higher compared to the routes G–H and C–D for the reason mentioned earlier, in Section V-A1. The rms delay spread shown in Fig. 10(b) is better predicted by using the correct corner shape and $\varepsilon_r = 2$. Predictions made with the right angle wedge shape give a much higher delay spread in the region from 20 to 70 m, while predictions made with $\varepsilon_r = 6$ are generally too low.

For comparison, the mean and standard deviation of the prediction errors of the signal power and rms delay spread are listed in Table III for both shapes of building corner and both values of ε_r. From the results listed, we conclude that the corner shape has clear influence on the prediction of the received power and the rms delay spread. It is seen that the influence on the prediction of the received power is greater than on the prediction of the rms delay spread. This result emphasizes the importance of the accuracy of the shape of the building corners and their electrical properties for accurate predictions. Our studies have also shown that the position of the corner is very important. Since the corner acts as a reflector, inaccuracy of its position relative to other corners at the intersection may lead to the prediction of high reflected power along the OOS street.

VII. CONCLUSION

This paper has presented results showing the influence of the diffraction coefficient and the shape and electrical properties of building corners on the prediction of received power and the rms delay spread in a microcellular environment. In order to overcome the limitations of the existing heuristic diffraction coefficient used in ray tracing programs, a new heuristic diffraction coefficient has been developed. The NHDC has higher diffracted field in deep shadow and eliminates the dips in the diffracted field that appear in the LHDC. Comparison of the results obtained from the VPL ray tracing tool using NHDC and the current heuristic diffraction coefficient are made with measurement results from different path types in a small cell. The use of the NHDC results in a more accurate power predictions in the shadow regions, where power predictions have historically been more pessimistic when compared to the measurements. The influence of the shape of the building corner on the ray tracing prediction has been investigated. The corner shape has an important role in the coupled field strength in OOS propagation. It has been shown that a detailed representation of the corner can be important for accurate prediction of both received power and delay spread. As future work; a detailed study on the influence of database of the large building entrance on propagation characteristics, since they are usually not included in the database.

ACKNOWLEDGMENT

The first author would like to thank Prof. Antti Räisänen for his encouragement. The authors would like to thank the measurement team at Radio Laboratory, Institute of Digital Communication (IDC) at HUT for conducting the measurements. The authors appreciate reviewers, comments that improved the paper.

REFERENCES

[1] M. C. Lawton and J. P. McGeehan, "The application of a deterministic ray launching algorithm for the prediction of radio channel characteristics in small-cell environments," *IEEE Trans. Veh. Technol.*, vol. 43, pp. 955–969, Nov. 1994.

[2] G. E. Athanasiadou, A. R. Nix, and J. P. McGeehan, "A microcellular ray tracing model and evaluation of its narrow-band and wide-band predictions," *IEEE J. Select. Areas Commun.*, vol. 18, pp. 322–355, Mar. 2000.

[3] G. Liang and H. Bertoni, "A new approach to 3-D ray tracing for propagation prediction in cities," *IEEE Trans. Antennas Propagat.*, vol. 46, pp. 853–863, June 1998.

[4] J. P. Rossi, J. C. Bic, A. J. Levy, Y. Gabillet, and M. Rosan, "A ray launching method for radio mobile propagation in urban area," in *Proc. IEEE Antennas and Propagation Society Symp. Dig.*, vol. 3, June 24–28, 1991, pp. 1540–1543.

[5] S. Y. Tan and H. S. Tan, "A microcellular communications propagation model based on the uniform theory of diffraction and multiple image theory," *IEEE Trans. Antennas Propagat.*, vol. 44, pp. 1317–1326, Oct. 1996.

[6] K. Rizk, J.-F. Wagen, and F. Gardiol, "Two-dimensional ray tracing modeling for propagation in microcellular environments," *IEEE Trans. Veh. Technol.*, vol. 46, pp. 508–518, May 1997.

[7] A. G. Kanatas, I. D. Kounouris, G. B. Kostaras, and P. Constantinou, "A UTD propagation model in urban microcellular environments," *IEEE Trans. Veh. Technol.*, vol. 46, pp. 185–193, Feb. 1997.

[8] V. Erceg, S. J. Fortune, J. Ling, A. J. Rustako, and R. A. Valenzuela, "Comparisons of a computer-based propagation prediction tool with experimental data collected in urban microcellular environments," *IEEE J. Select. Areas Commun.*, vol. 15, pp. 677–684, May 1997.

[9] H. R. Anderson, "A ray tracing propagation model for digital broadcasting systems in urban areas," *IEEE Trans. Broadcasting*, vol. 39, pp. 309–317, Sept. 1993.

[10] R. G. Kouyoumjian and P. H. Pathak, "A uniform geometrical theory of diffraction for and edge in a perfectly conducting surface," *Proc. IEEE*, vol. 62, pp. 1448–1461, Nov. 1974.

[11] D. A. McNamara, C. W. I. Pistorius, and J. A. G. Malherbe, *Introduction to the Uniform Geometrical Theory of Diffraction*. Norwood, MA: Artech House, 1996.

[12] L. B. Felsen and N. Marcuvitz, *Radiation and Scattering of Waves*. Englewood Cliffs, NJ: Prentice-Hall, 1973.

[13] R. G. Rojas, "Electromagnetic diffraction of an obliquely incident plane wave field by a wedge with impedance faces," *IEEE Trans. Antennas Propagat.*, vol. 36, pp. 956–970, July 1988.

[14] R. Tiberio, G. Pelosi, G. Manara, and P. H. Pathak, "High-frequency scattering from a wedge with impedance faces illuminated by a line source—Part I: Diffraction," *IEEE Trans. Antennas Propagat.*, vol. 37, pp. 212–218, Feb. 1989.

[15] G. Pelosi, G. Manara, and P. Nepa, "Diffraction by a wedge with variable-impedance faces," *IEEE Trans. Antennas Propagat.*, vol. 44, pp. 1334–1340, Oct. 1996.
[16] M. F. Otero and R. G. Rojas, "Two-dimensional Green's function for a wedge with impedance faces," *IEEE Trans. Antennas Propagat.*, vol. 45, pp. 1799–1809, Dec. 1997.
[17] G. D. Maliuzhinets, "Excitation, reflection and emssion of surface waves from a wedge with given face impedances," *Sov. Phys. Dokl.*, vol. 3, pp. 752–755, 1958.
[18] R. J. Luebbers, "Finite conductivity uniform UTD versus knife diffraction prediction of propagation path loss," *IEEE Trans. Antennas Propagat.*, vol. AP-32, pp. 70–76, Jan. 1984.
[19] K. A. Remely, H. R. Anderson, and A. Weisshar, "Improving the accuracy of ray tracing techniques for indoor propagation modeling," *IEEE Trans. Veh. Technol.*, vol. 49, pp. 2350–2357, Nov. 2000.
[20] ——, "Improved diffraction coefficients for lossy dielectric wedges," *Electron. Lett.*, vol. 35, no. 21, pp. 1826–1827, Oct. 1999.
[21] P. D. Holm, "A new heuristic UTD diffraction coefficient for nonperfectly conducting wedges," *IEEE Trans. Antennas Propagat.*, vol. 48, pp. 1211–1219, Aug. 2000.
[22] A. Taflove, *Computational Electrodynamics: The Finite-Difference Time-Domain Method*. Norwood, MA: Artech House, 1995.
[23] K. Kalliola, J. Laurila, M. Toeltsch, K. Hughl, P. Vainikainen, and E. Bonek, "3-D directional wideband dual-polarized measurement of urban mobile radio channel with synthetic aperture technique," presented at the AP2000 Millennium Conference on Antennas and Propagation, Davos, Switzerland, Apr. 2000, pp. 9–14.
[24] J. Kivinen, T. Korhonen, P. Aikio, R. Gruber, P. Vainikainen, and S.-G. Haggman, "Wideband radio channel measurement system at 2 GHz," *IEEE Trans. Instrum. Meas.*, vol. 48, pp. 39–44, Feb. 1999.
[25] O. Landron, M. J. Feuerstein, and T. S. Rappaport, "A comparison of theoretical and empirical reflection coefficients for typical exterior wall surfaces in mobile radio environment," *IEEE Trans. Antennas Propagat.*, vol. 44, pp. 341–351, Mar. 1996.
[26] R. J. Luebbers, W. A. Foose, and G. Reyner, "Comparison of GTD propagation model wide-band path loss simulation with measurements," *IEEE Trans. Antennas Propagat.*, vol. 37, pp. 499–505, Apr. 1989.
[27] J. Kivinen, X. Zhao, and P. Vainikainen, "Empirical characterization of wideband indoor radio channel at 5.3 GHz," *IEEE Trans. Antennas Propagat.*, vol. 49, pp. 1192–1203, Aug. 2001.
[28] H. L. Bertoni, *Radio Propagation for Modern Wireless Systems*. Englewood Cliffs, NJ: Prentice-Hall, 2000.
[29] K. Rizk, J.-F. Wagen, and F. Gardiol, "Influence of database accuracy on two-dimensional ray tracing based prediction in urban microcells," *IEEE Trans. Veh. Technol.*, vol. 49, pp. 631–642, Mar. 2000.

Hassan M. El-Sallabi (S'99) received the B.Sc. (with honors) and M.Sc. degrees from Garyounis University, Benghazi, Libya, both in electrical engineering. He received the Licentiate of Technology degree from Helsinki University of Technology (HUT), Espoo, Finland, in Feb. 2000. He is currently working toward the D.Sc. degree at HUT.

From 1988 to 1996, he was a Telecommunications Engineer with General Electric Company, Benghazi, Libya. From 1996 to 1997, he was an Assistant Lecturer, Department of Electrical Engineering, Garyounis University, Benghazi, Libya. Since 1997, he has been a Research Engineer, with the Radio Laboratory, HUT. His current research interests include wide-band propagation modeling and channel characterization for microcellular mobile communications.

George Liang (S'89-M'91) received the B.S. degree in electrical engineering from the University of British Columbia, Vancouver, BC, Canada, the M.S. degree in electrophysics and Ph.D. degree in electrical engineering, both from Polytechnic University, Brooklyn, NY, in 1991, 1995, and 1997, respectively.

From 1991 to 1994, he was a Network Engineer, at Timber Hill, Inc. In 1994, he joined the propagation prediction group as a Research Assistant, at the Polytechnic University. In 1997, he cofounded SiteWare Technologies, Inc., and has been the President and Principle Researcher since that time. His research interests include the development of a full function propagation prediction software tools for mobile and wireless communications.

Henry L. Bertoni (M'67-SM'79-F'87) received the B.S. degree in electrical engineering from Northwestern University, Evanston, IL., the M.S. degree also in electrical engineering and the Ph.D. degree in electrophysics, both from the Polytechnic Institute of Brooklyn (now Polytechnic University), Brooklyn, NY, in 1960, 1962, and 1967, respectively.

In 1990, he joined the Faculty of the Polytechnic University; since 2001, he has been Head of the Electrical and Computer Engineering CE Department and from 1995 to 1996, he served as Vice Provost of the Graduate Studies Program. His research interests includes theoretical aspects of wave phenomena in electromagnetics, ultrasonics, acoustics, and optics. He has authored or coauthored over 75 journal papers and 9 book chapters. Four journal articles have received best paper awards. From 1982 to 1983, he spent a sabbatical leave at University College London, U.K., as a Guest Research Fellow of the Royal Society. His current research in electromagnetics deals with the theoretical prediction of UHF propagation characteristics in urban environments. He and his students were the first to explain the mechanisms underlying characteristics observed for propagation of the cellular mobile radio signals. Much of this work is described in his recent book *Radio Propagation for Modern Wireless Systems*, (New York: Prentice-Hall, 2000.

Dr. Bertoni was the first Chairman of the Technical Committee on Personal Communications of the IEEE Communications Society, and was IEEE representative to, and chairman of the Hoover Medal Board of Award. He has served on the ADCOM of the IEEE Ultrasonics, Ferroelectric, and Frequency Control Society, and is a member of the International Scientific Radio Union and the Radio Club of America. From 1998 to 2001, he was a Distinguished Lecturer of the IEEE Antennas and Propagation Society.

Ioannis T. Rekanos (S'92-A'00-M'02) was born in Thessaloniki, Greece, in 1970. He received the Dipl.Eng. degree (with honors) in electrical engineering, and the Dr.Eng. degree in electrical and computer engineering, both from the Aristotle University of Thessaloniki (AUTH), Greece, in 1993 and 1998, respectively.

From 1993 to 1998, he was a Research and Teaching Assistant in the Department of Electrical and Computer Engineering at AUTH. Since 2000, he has been with the Radio Laboratory at the Helsinki University of Technology, Finland, where he is currently a Senior Researcher holding a Marie Curie Postdoctoral Fellowship. His research interests include inverse electromagnetic problems, computational electromagnetics, optimization techniques, and neural network applications in electromagnetics.

Dr. Rekanos has been a scholar of the Bodossaki Foundation, Greece. He is a member of the American Geophysical Union, the Marie Curie Fellowship Association, and the Technical Chamber of Greece. In 1995, he received the URSI, Commission B, Young Scientist Award.

Pertti Vainikainen (S'87-M'90) was born in Helsinki, Finland, in 1957. He received the M.Sc., Licentiate of Sci., and D.Sc. degrees, all in technology, from Helsinki University of Technology (HUT), Espoo, Finland, in 1982, 1989, and 1991, respectively.

From 1981 to 1992, he was a Teaching Assistant and Researcher with the Radio Laboratory of HUT. From 1992 to 1993, he was an Acting Professor of Radio Engineering; from 1993 to 1998, he was an Associate Professor of Radio Engineering; and and since 1998, he has been a full Professor in Radio Engineering, at the Radio Laboratory of HUT. From 1993 to 1997, he was Director of the Institute of Radio Communications (IRC) of HUT. He is the author or coauthor of three books and about 110 refereed international journal or conference publications. He has received four patents. His research interests include RF techniques in radio communications and industrial measurement applications of radio waves.